J Appl Electrochem (2012) 42:953–959
DOI 10.1007/s10800-012-0462-9

ORIGINAL PAPER

Performance enhancement of strontium-doped lanthanum manganite cathode by developing a highly porous microstructure

Dhruba Panthi · Bokkyu Choi · Atsushi Tsutsumi

Received: 16 May 2012 / Accepted: 22 July 2012 / Published online: 5 August 2012

Abstract A simple and promising template method was applied for the development of a highly porous microstructure, referred to as a macroporous structure (having pore size >50 nm), for a solid oxide fuel cell strontium-doped lanthanum manganite (LSM) cathode. Using poly(methyl methacrylate) beads of 2.9 μm size as the pore-forming templates, a porosity value of ca. 63 % was achieved. The electrochemical performance of the developed macroporous cathode was evaluated by measuring electrochemical impedance spectra of the symmetrical cells as well as power density of the full cells. The results indicated that due to enhanced oxygen diffusion and reaction kinetics, the macroporous structure was effective in reducing the interfacial polarization resistance of the LSM cathode and hence attaining a higher cell performance.

Keywords Solid oxide fuel cell · Strontium-doped lanthanum manganite cathode · Macroporous structure · Template method

1 Introduction

Solid oxide fuel cells (SOFCs) are regarded as one of the most promising electrochemical devices for power generation due to their numerous favorable characteristics such as high energy conversion efficiency, ability to run on direct hydrocarbon fuels, and possibility of utilizing high-exergy waste heat in combined cycle applications [1–7]. Moreover, SOFC components can be fabricated from easily obtainable ceramic materials, thus avoiding the use of precious noble metals that may be subjected to resource constraints for mass production. State-of-the-art SOFCs make use of 8 mol.% yttria-stabilized zirconia (YSZ), Ni-YSZ cermet and strontium-doped lanthanum manganite (LSM) as electrolyte, anode, and cathode, respectively. However, one of the major challenges for the widespread deployment of SOFCs has been found to be the limitations posed by oxygen reduction reactions (ORR) occurring at the LSM cathode [8–10].

LSM has traditionally been a preferred material for SOFC cathode due to its good compatibility with zirconia-based electrolytes as well as thermal/chemical stability in oxidizing environments. However, the polarization resistance of a LSM cathode is substantially high owing to its poor ionic conductivity. LSM has been reported to have an ionic conductivity of 10^{-7}–10^{-6} S cm^{-1} in the temperature range 900–1,000 °C, over eight orders of magnitude less than its electronic conductivity [11]. The ionic conductivity of LSM becomes even poorer with decreasing temperature, thereby limiting electrochemical reactions to the three-phase boundary (TPB) regions where electrode, electrolyte, and gas phases meet [12]. In an effort to address issues related to conventional LSM cathodes, mixed ionic-electronic conducting (MIEC) materials, such as strontium-doped lanthanum ferrite (LSF) and strontium-doped lanthanum cobalt ferrite (LSCF), have been proposed as alternative cathodes [12–14]. However, these MIEC cathodes cause problems due to their reactivity and/or unmatched coefficient of thermal expansion (CTE) with the most widely used YSZ electrolytes. As a result, they require a protective interlayer, usually of samaria-doped ceria (SDC) or gadolinia-doped ceria (GDC), when used with YSZ electrolytes [15, 16], which in turn makes the manufacturing process complex and costly. Therefore, enhancement of the performance of LSM

D. Panthi · B. Choi · A. Tsutsumi (✉)
Collaborative Research Center for Energy Engineering, Institute of Industrial Science, The University of Tokyo, 4-6-1 Komaba, Meguro-ku, Tokyo 153-8505, Japan
e-mail: a-tsu2mi@iis.u-tokyo.ac.jp

or LSM-based cathodes would be a more desirable approach, particularly for SOFCs operating in the temperature range 700–900 °C [14].

Porosity is a key microstructural characteristic that is known to play a prominent role in determining the performance of SOFC electrodes, including LSM cathodes [17, 18]. Conventionally, pore formers, such as carbon black, graphite, cellulose, or starch, are employed to render porosity in SOFC electrodes [19–21]. However, the porosity obtained in this way is often random with non-uniform geometry and low specific surface area. Precise tailoring of the porosity to give well-defined geometry and larger specific surface area is thus desirable. Proper control of the porosity is considered to improve electrode performance by both facilitating the diffusion of gaseous species and increasing the active surface area for electrochemical reactions to take place. As a result, macroporous or multi-scale porous electrodes have recently been the subject of investigation of several research groups.

Colloidal-crystal templating method was employed by Chen et al. [22] to prepare a three-dimensionally ordered macroporous (3DOM) strontium-doped samarium cobaltite (SSC) cathode using polystyrene (PS) spheres as templating materials. Marrero-López et al. [20] also followed the approach of colloidal-crystal templating to develop a number of 3DOM materials for SOFC components. Although 3DOM structures seem promising for optimizing SOFC performance, they suffer from two issues [23]: (i) SOFC electrodes usually consist of composite materials, hence it is quite challenging to achieve the desired stoichiometry from a solution containing more than one metal precursor; (ii) due to very thin walls in the final structure, it is often difficult to retain macroporosity at temperatures high enough for SOFC operation. To deal with these issues, alternative routes have also been investigated by some researchers. Zhang et al. [23] prepared a SSC–GDC cathode and NiO–GDC anode with combined meso-/macroporous structure by applying a foam of poly(methyl methacrylate) (PMMA) beads as the template. Several SOFC components with macroporous structures have been developed by Ruiz-Morales et al. [24] using PMMA pore formers in a polyvinyl alcohol (PVA) solution. In addition, an encouraging performance of micro-tubular SOFC was achieved by Suzuki et al. [25] by engineering the anode microstructure with PMMA beads.

Despite a considerable amount of literature on the development of macroporous SOFC components, little work has been focused particularly on the role of macroporous structure for the promotion of ORR at the LSM cathode. It is also critical to figure out the reasonable range of SOFC operating temperature so as to achieve the optimum benefit of macroporous LSM cathode. Therefore, the present research aims to systematically investigate the effect of macroporous structure on the electrochemical characteristics of the LSM cathode.

2 Experimental

2.1 Preparation of SOFC button cells

SOFC button cells with two types of cathode microstructures were prepared as described below. To focus the investigations on cathode microstructure, the same anode microstructure was used for both types of samples.

2.1.1 Samples with macroporous cathode microstructure

Macroporous cathode samples were fabricated using LSM nanopowder with an average particle size of 60 nm (Na-Bond Technologies, China) and PMMA microspheres of 2.9 μm size (Soken Chemical and Engineering, Japan), as illustrated in Fig. 1a. Although both PS and PMMA are widely used for developing macroporous microstructures, PMMA was selected in this study because of its better wettability with polar solvents like PVA, and better combustion properties than PS [26]. The cathode slurry was prepared by mixing 5 g of LSM nanopowder with an equal amount of PMMA in a 6 wt% PVA (Sigma-Aldrich, Germany) solution (water-based) with the help of a magnetic stirrer.

To fabricate the symmetrical cells for half-cell impedance tests, the cathode slurry was screen-printed on both

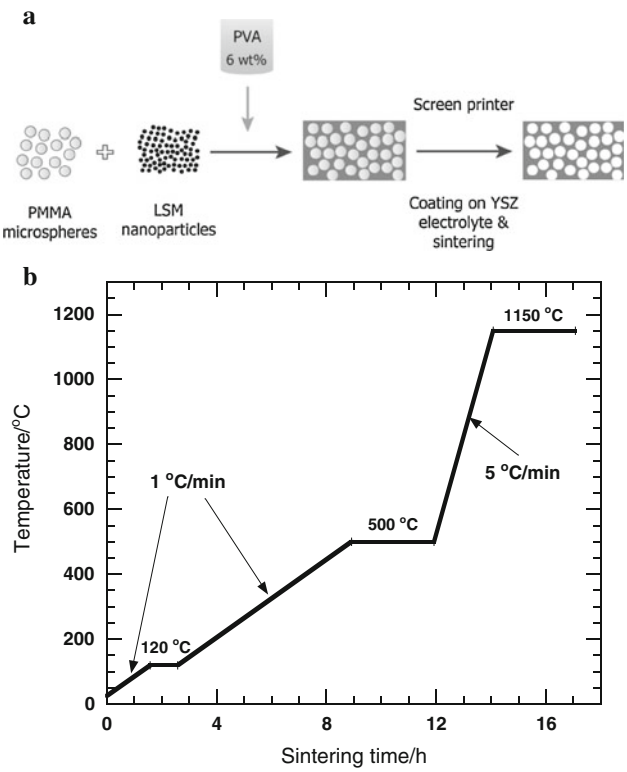

Fig. 1 Fabrication of the macroporous cathode by template method: **a** process flow diagram and **b** temperature profile for sintering

sides of the 8 mol.% YSZ electrolytes (Japan Fine Ceramics, Japan), which had a diameter of 20 mm and an approximate thickness of 300 μm. The thickness of the electrodes was maintained at ca. 50 μm. The screen-printed samples were sintered in air at 1,150 °C following a temperature profile as shown in Fig. 1b. The samples were first heated at a relatively slow rate and held at 120 °C (around which the melting of PMMA starts) for 1 h and at 500 °C (around which complete burning out of PMMA takes place) for 3 h, so as to release the vapor of PMMA particles in a smooth way while maintaining the templated porosity without much shrinkage or collapse in the microstructure.

To perform the single cell tests, full cells were fabricated by screen-printing the anode slurry on one side of the YSZ electrolytes and the cathode slurry on the other side. To prepare the anode slurry, 6 g of NiO powder (Wako Pure Chemical, Japan) and 4 g of YSZ powder with an average particle size of 0.5 μm (Daiichi Kigenso Kagaku Kogyo, Japan) were mixed in terpineol solvent (Wako Pure Chemical, Japan). 0.2 g of ethyl cellulose (Kanto Chemical, Japan) and 1 g of Avicel (monocrystalline cellulose) (Merck, Germany) were used as the binder and the pore former, respectively. The mixture was then ball milled in zirconia media for 24 h until a homogenous slurry was obtained. Sintering of the anode side was carried out in air by heating the screen-printed samples at a rate of 5 °C min^{-1} up to 1,400 °C and then holding at that temperature for 1 h.

2.1.2 Samples with conventional cathode microstructure

To compare the performance of the macroporous cathode, SOFC button cells with conventional cathode microstructures were also fabricated. For these samples, the cathode slurry was prepared by mixing 10 g of micro-scale LSM powder with an average particle size of 2.48 μm (Daiichi Kigenso Kagaku Kogyo, Japan) in terpineol solvent (Wako Pure Chemical, Japan) with 0.2 g of ethyl cellulose binder (Kanto Chemical, Japan) and 1 g of Avicel pore former (Merck, Germany). The slurry was then screen-printed on the YSZ electrolytes, and the samples were sintered by heating at a rate of 5 °C min^{-1} up to 1,150 °C and then holding at that temperature for 3 h.

For the full cells, the preparation method for the anode was the same as for the first type of samples.

2.2 Experimental setup

The SOFC test setup used for the evaluation of the performance of the SOFC button cells is shown in Fig. 2. The button cell was placed above a cell support tube made of alumina. A glass O-ring was used to provide high-temperature gas-tight sealing between the anode and cathode

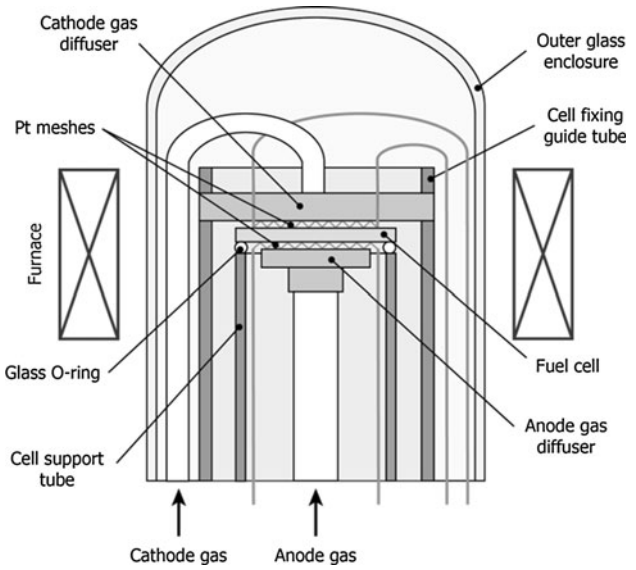

Fig. 2 Schematic of the test setup for evaluating SOFC button cells

gases, and the cell was fixed in place from the upper side with a cell fixing guide tube. The anode gas was supplied from the bottom (inner) side of the cell while the cathode gas was supplied from the top (outer) side of the cell through glass tubes. Platinum meshes were used to collect current from both electrodes of the cell and a four-probe technique was employed to measure the current and voltage across the cell.

An electric furnace was used to heat the samples to the required testing temperatures. The samples were heated at a rate of 5 °C min^{-1} up to 900 °C, at which temperature the glass O-ring melted down and provided the necessary sealing. The performance measurements were made at 900 °C and lower temperatures by reducing the furnace temperature at a rate of 3 °C min^{-1}.

2.3 Electrochemical performance evaluation

The performance of the symmetrical cells was evaluated by recording their electrochemical impedance spectra (EIS) with pure oxygen (50 cm^3 min^{-1} each) supplied to both the electrodes. An AC amplitude of 20 mV was applied within a frequency range 100 kHz–0.1 Hz under OCV conditions. Area-specific resistance, R_p, was determined from the difference of the low- and high-frequency intercepts on the real axis.

Single cell performance was evaluated by potentiodynamic measurements with a supply of humidified hydrogen containing about 3 % steam (50 cm^3 min^{-1}) as the fuel and pure oxygen (50 cm^3 min^{-1}) as the oxidant. Because the electrochemical performance of a LSM cathode is known to improve with initial current passage through it as a result of the activation effect [27], the cells were treated

with a cathodic current of 100 mA cm^{-2} for half an hour before electrochemical measurements.

2.4 Microstructure characterization

Microstructures of the SOFC cathodes were examined with scanning electron microscope (SEM) micrographs (JSM-7001F, JEOL, Japan).

Porosimetry data for the two types of cathode structures were obtained following two different methods due to the different nature of their porosities. To characterize the macroporous cathode structure with high porosity, mercury intrusion data were obtained with a mercury porosimeter (AutoPore IV 9500 V1.07, Micromeritics Instrument, USA). In contrast, nitrogen adsorption isotherms determined with a vapor adsorption apparatus (Belsorp 18, Nihon Bel, Japan) were used to characterize the porous structure of the conventionally prepared cathode that contained relatively low porosity and only micro- and meso-scale pores.

3 Results and discussion

SEM images of macroporous and conventional LSM cathodes before the electrochemical tests were performed are shown in Fig. 3a, b, respectively. A typical honeycomb like appearance of the macroporous cathode, depicting the porosity rendered by the PMMA templates, can be observed in Fig. 3a. On the other hand, a more packed microstructure of the conventional cathode is observed in Fig. 3b. Close-up views of the pores present in the two types of cathode can be compared in Fig. 3c, d. The macroporous cathode shows significantly high porosity with well-defined pores. However, the mean pore size was observed to be slightly less than 2 μm, against the original template size of 2.9 μm. Thus, appreciable shrinkage is evident in the size of the templated pores.

The total intrusion volume and total pore area of the macroporous cathode were shown to be 0.665 cm^3 g^{-1} and 1.44 m^2 g^{-1}, respectively. Figure 4 illustrates the distribution of pore sizes for the same cathode by the plotting of cumulative and differential intrusions against pore diameter. The cumulative intrusion curve begins to increase from the pore diameter of 2.48 μm and is almost saturated when it reaches the pore diameter of 0.22 μm. From the differential intrusion curve, the highest pore volume can clearly be observed at the pore diameter of 1.92 μm. The average pore diameter for the macroporous cathode was estimated to be 1.85 μm, which is only 64 % of the size of the PMMA templates used (2.9 μm). This corresponds with the SEM observation of the macropores. Although the temperature profile for sintering was chosen carefully, the microstructure suffered significant shrinkage, probably due

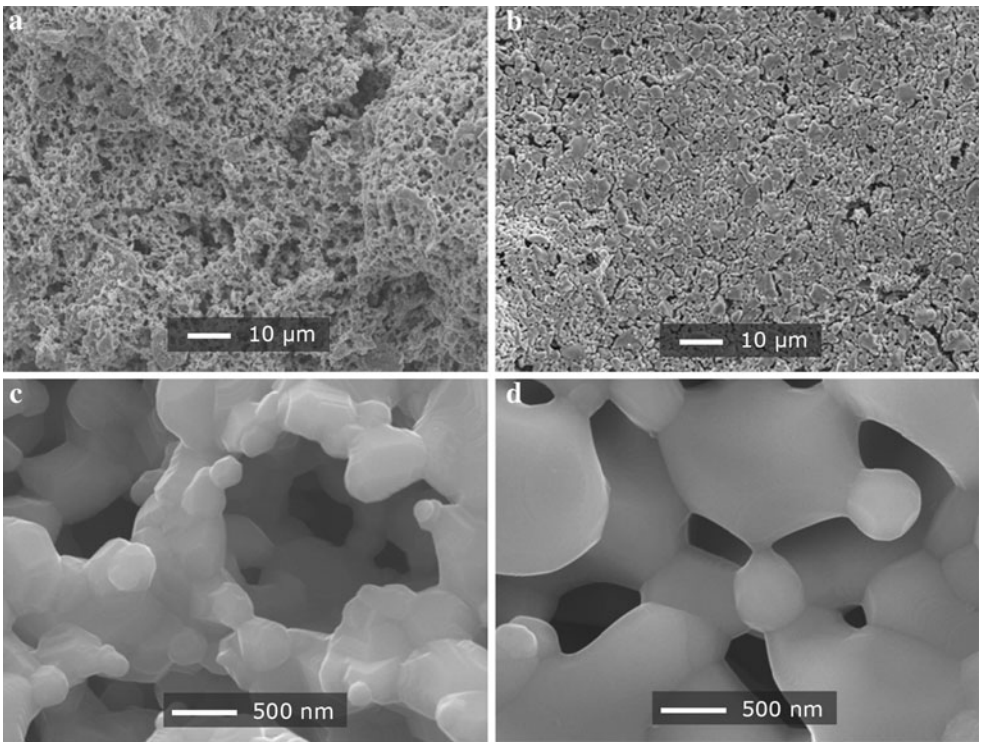

Fig. 3 SEM micrographs: **a** macroporous LSM cathode, **b** conventional LSM cathode, **c** close-up view of the pores in macroporous cathode, and **d** close-up view of the pores in conventional cathode

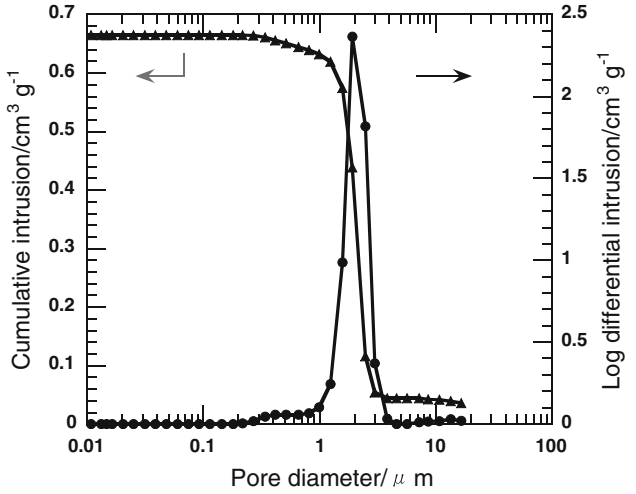

Fig. 4 Cumulative and differential pore volumes as a function of pore size for the macroporous cathode

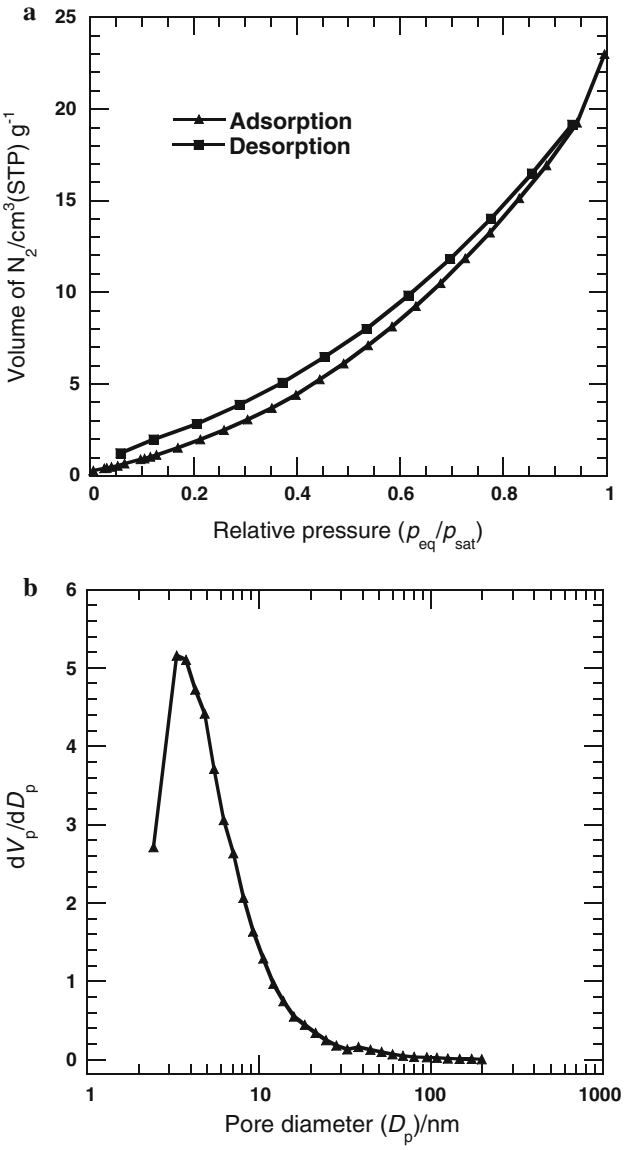

Fig. 5 Porosimetry analysis of the conventional cathode: **a** nitrogen adsorption/desorption isotherms and **b** BJH pore size distribution plot

to the rather high sintering temperature. Nevertheless, the porosity value obtained (ca. 63 %) can be considered to be suitably high enough for the SOFC cathode.

For the conventional cathode, a total pore volume of 0.0415 cm^3 g^{-1} and a BET surface of 25.68 m^2 g^{-1} were obtained. Nitrogen adsorption/desorption isotherms measured at 77 K and the BJH pore size distribution plot corresponding to the adsorption data for the conventional cathode are shown in Fig. 5a, b, respectively. As can be observed from the BJH plot, the peak pore diameter for the conventional cathode was 3.32 nm. In addition, since the pore size distribution was only in the microporous to mesoporous range, it is probable that the porous structure achieved through the conventional approach was not sufficient when it comes to facilitating the gaseous diffusion through the LSM cathode.

Considering the fact that single-phase LSM cathodes are primarily intended for high-temperature applications, a temperature range 800–900 °C was chosen for the electrochemical measurements. Nyquist plots recorded for the symmetrical cells with macroporous and conventional cathodes are shown in Fig. 6. In these plots, the difference of the low- and high-frequency intercepts on the real axis gives the area-specific interfacial polarization resistance corresponding to two half cells in series (i.e., $2R_p$). The values of R_p at different temperatures for both macroporous and conventional samples are listed in Table 1. At 900 °C, the values of R_p were 2.33 and 1.26 Ω cm^2 for conventional and macroporous cathodes, respectively. This implies that the polarization resistance was reduced by 46 % when the cathode microstructure was switched from a conventional one to a macroporous one. Similarly, the values of R_p were measured as 5.1 and 11.63 Ω cm^2 for the conventional cathodes at 850 and 800 °C, respectively. With the macroporous cathode structure, these values were reduced, respectively, to 3.12 and 8.42 Ω cm^2, entailing a reduction of 39 and 28 % in the interfacial polarization resistance. Thus, it can be concluded that the templated porous microstructure was effective in reducing the interfacial polarization resistance of the LSM cathode. The macroporous structure is likely to have considerably improved the diffusion kinetics and electrochemical activity of the LSM cathode leading to a decrease in the polarization losses. The sufficiently large pore sizes in the macroporous structure resulted in a framework of well-connected open pores thereby promoting the transport of oxygen and reaction products through the cathode. On the other hand, the increased total porosity of the macroporous

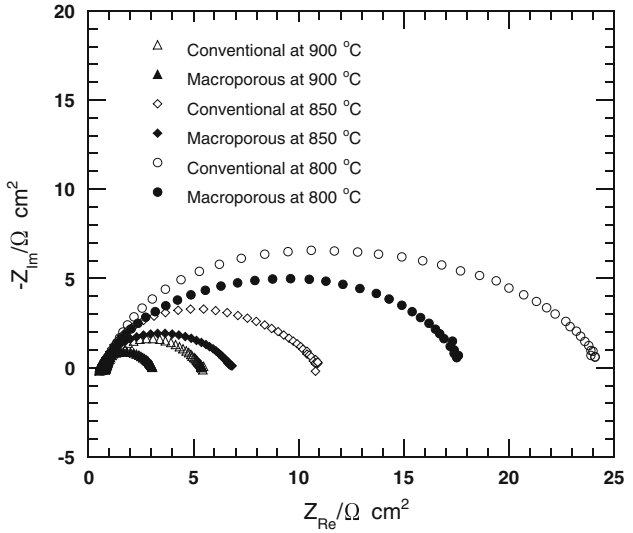

Fig. 6 Nyquist plots for symmetrical cells with macroporous and conventional cathodes

Table 1 Area-specific resistances corresponding to cathodic half cells

Cathode structure	Area-specific resistance (R_p Ω cm^2)		
	900 °C	850 °C	800 °C
Macroporous	1.26	3.12	8.42
Conventional	2.33	5.1	11.63

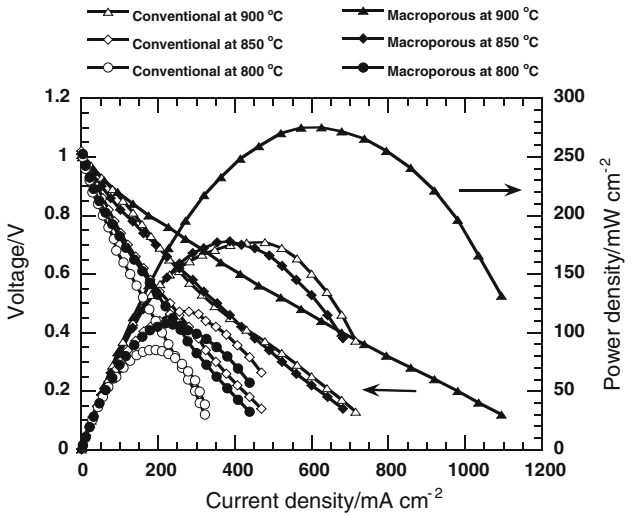

Fig. 7 Voltage–current performance for single cells with macroporous and conventional cathodes

structure provided a larger surface area for the ORR to take place.

Figure 7 shows the plots of cell voltage and power density as a function of the current density for electrolyte-supported full cells with both types of cathode microstructures. It can be observed that the maximum power density generated at 900 °C for the cell with the conventional cathode was 177 mW cm^{-2}, rising by 55 % to a value of 275 mW cm^{-2} for the cell with the macroporous cathode. At 850 °C, the macroporous cathode structure resulted in the maximum power density of 178 mW cm^{-2} which was 51 % high compared to that with the conventional cathode structure. Likewise, the maximum power densities achieved at 800 °C were 85 and 108 mW cm^{-2} for the cells with conventional and macroporous cathodes, respectively, implying an improvement of 27 % in the performance of the cell with the macroporous cathode. Thus, by and large, the results obtained from the single cell tests are consistent with those obtained from the symmetrical cell tests. Moreover, the contribution of electrochemical kinetics at the cathode to the overall cell performance confirms the dominance of cathode overpotential in SOFC voltage losses.

It is apparent from both symmetrical cell and single cell test results that the improvement achieved through the macroporous structure is more prominent at higher operating temperatures. This kind of temperature dependence of the improvement brought about by the macroporous cathode structure could be explained by the inherent property of the LSM material itself, as discussed in the "Introduction" section. Because the ionic conductivity of LSM reduces sharply with decrease in temperature, it has recently been a common approach to prepare composite cathodes by adding ionically conducting oxides such as YSZ and GDC to LSM to improve the ionic transport properties for the operation of SOFCs typically at or below 800 °C [28–30]. Thus, with the single-phase LSM cathode, the very low ionic conductivity of LSM at lower temperatures is likely to put a limit on its enhanced electrochemical activity despite the presence of a sufficiently high porosity.

4 Conclusions

It has been demonstrated that the development of the present macroporous structure is an effective approach to reduce the interfacial polarization resistance of the LSM cathode and hence attain a higher cell performance. The power density of SOFC button cells at 900 °C was found to increase by up to 55 % when the macroporous cathode structure was used. Although the cell performance was observed to improve considerably at all cell operating temperatures chosen in this study, the improvement was more pronounced at higher temperatures probably due to the limit set by the very low ionic conductivity of LSM at lower temperatures.

Acknowledgments The authors would like to thank Assoc. Prof. Guoqing Guan of Hirosaki University for his useful advice. The first author (D. Panthi) gratefully acknowledges the scholarship from the Ministry of Education, Culture, Sports, Science and Technology (MEXT) of Japan during the period of research.

References

1. Yamamoto O (2000) Electrochim Acta 45:2423
2. Steele BCH, Heinzel A (2001) Nature 414:345
3. Stambouli AB, Traversa E (2002) Renew Sustain Energy Rev 6:433
4. Ormerod RM (2003) Chem Soc Rev 32:17
5. Kuchonthara P, Bhattacharya S, Tsutsumi A (2003) J Power Sources 117:7
6. Kuchonthara P, Bhattacharya S, Tsutsumi A (2003) J Power Sources 124:65
7. Kuchonthara P, Bhattacharya S, Tsutsumi A (2005) Fuel 84:1019
8. Adler SB (2004) Chem Rev 104:4791
9. Weber A, Ivers-Tiffée E (2004) J Power Sources 127:273
10. Singhal SC, Wachsman ED (2009) Electrochem Soc Interface 18:38
11. Yasuda I, Ogasawara K, Hishinuma M, Kawada T, Dokiya M (1996) Solid State Ion 86:1197
12. Sun C, Hui R, Roller J (2010) J Solid State Electrochem 14:1125
13. Wincewicz K, Cooper J (2005) J Power Sources 140:280
14. Jacobson AJ (2010) Chem Mater 22:660
15. Simner SP, Bonnett JF, Canfield NL, Meinhardt KD, Shelton JP, Sprenkle VL, Stevenson JW (2003) J Power Sources 113:1
16. Mai A, Haanappel VAC, Uhlenbruck S, Tietz F, Stöver D (2005) Solid State Ion 176:1341
17. Virkar AV, Chen J, Tanner CW, Kim J-W (2000) Solid State Ion 131:189
18. Ruiz-Morales JC, Marrero-López D, Gálvez-Sánchez M, Canales-Vázquez J, Savaniu C, Savvin SN (2010) Energy Environ Sci 3:1670
19. Yoon KJ, Huang W, Ye G, Gopalan S, Pal UB, Seccombe DA Jr (2007) J Electrochem Soc 154:B389
20. Marrero-López D, Ruiz-Morales JC, Peña-Martínez J, Canales-Vázquez J, Núñez P (2008) J Solid State Chem 181:685
21. Nie L, Liu J, Zhang Y, Liu M (2011) J Power Sources 196:9975
22. Chen F, Xia C, Liu M (2001) Chem Lett 30:1032
23. Zhang Y, Zha S, Liu M (2005) Adv Mater 17:487
24. Ruiz-Morales JC, Canales-Vázquez J, Peña-Martínez J, Marrero-López D, Irvine JTS, Núñez P (2006) J Mater Chem 16:540
25. Suzuki T, Hasan Z, Funahashi Y, Yamaguchi T, Fujishiro Y, Awano M (2009) Science 325:852
26. Sadakane M, Asanuma T, Kubo J, Ueda W (2005) Chem Mater 17:3546
27. Jiang SP (2005) J Solid State Electrochem 11:93
28. Barbucci A, Viviani M, Panizza M, Delucchi M, Cericola G (2005) J Appl Electrochem 35:399
29. Deseure J, Bultel Y, Dessemond L, Siebert E, Ozil P (2007) J Appl Electrochem 37:129
30. Jiang SP (2008) J Mater Sci 43:6799